

Article

Not peer-reviewed version

The Fontanamare Discovery (Sardinia coast, Italy), A Case of Underwater Corrosion of Bronze Coins

[Tilde De Caro](#)*, Fiammetta Susanna, [Mauro Francesco La Russa](#), Andrea Macchia

Posted Date: 23 June 2023

doi: 10.20944/preprints202306.1692.v1

Keywords: bronze corrosion; submarine environment; Fontanamare wreck



Preprints.org is a free multidiscipline platform providing preprint service that is dedicated to making early versions of research outputs permanently available and citable. Preprints posted at Preprints.org appear in Web of Science, Crossref, Google Scholar, Scilit, Europe PMC.

Copyright: This is an open access article distributed under the Creative Commons Attribution License which permits unrestricted use, distribution, and reproduction in any medium, provided the original work is properly cited.

Article

The Fontanamare discovery (Sardinia coast, Italy), a case of underwater corrosion of bronze coins

Tilde de Caro ^{1*}, Fiammetta Susanna ², Mauro Francesco La Russa³ and Andrea Macchia ^{2,3}

1. CNR ISMN, Str Provinciale 35 n 9, I-00010 Rome, Italy; tilde.decaro@cnr.it

2. YOCOCU, Youth Conservat Cultural Heritage, Via T Tasso 108, I-00185 Rome, Italy; aps@yococu.com

3. DIBEST, University of Calabria, Via Pietro Bucci, 87036 Arcavacata CS, Italy; mlarussa@unical.it

* Correspondence: tilde.decaro@cnr.it;

Abstract: The study reported the analytical approach on nine coins found in the wreck A of Fontanamare for understanding the complex corrosion processes that take place in underwater conditions. Optical microscopy (OM), combined with micro-Raman (μ -Raman) spectroscopy, and X-ray diffractometry (XRD) and scanning electron microscopy with energy dispersive X-ray spectroscopy (SEM + EDS) were used to analyse the nature and the microstructure of the corrosion patina in comparison with the non-degraded state of coins. Three main type of corrosion patina based on copper, lead chloride and carbonate were identified: white-green, black and the obtained results for understanding the complex corrosion processes that take place in underwater conditions.

Keywords: bronze corrosion; submarine environment; Fontanamare wreck.

1. Introduction

This study is focused on the presentation and discussion of the analytical investigations carried out on nine coins found in the wreck A of Fontanamare, dated to the 3rd century AD, the defined Antoninian age. The Fontanamare site is in the Gonnese bay, located on the southwestern side of Sardinia, in the Iglesiente region. Sardinia was the centre of the routes between East and West as early as the 15th century. B.C. as evidenced by Mycenaean attestations, a strong presence of Cypriot materials followed in the 12th century B.C., which testify to exchanges with the Nuragic populations above all from the point of view of the copper trade and bronze working [1].

During underwater campaigns on the southwest coast of Sardinia, in front of Fontanamare (Figure 1A), first in 1965 and then again in 1972, three wrecks were identified and dated thanks to the find of numerous amphorae [2,3].

The geomorphological configuration of Fontanamare Bay is characterised by a series of rocks that extend beyond the rocky barrier that runs parallel to the coast between Porto Paglia and Fontanamare. This barrier, combined with the shallow depth of the sea in that stretch and a frontal exposure to the mistral wind and almost tangentially to the libeccio wind, has always posed a risk to navigation. Numerous wrecks that have sunk there have left behind materials that give an indication of this danger.

Wrecks and artefacts of the marine heritage were already known in the sixties of the past century and made the object of numerous depredations. Only between 1997 and 1999 did the Superintendence of Cagliari and Oristano conduct some underwater reconnaissance. The research focused on an area south of Sa Punta e S' Arena, extending northeast for one kilometre towards Fontanamare and north-west for about 350 m from the coastline (Figure 1A). The prospecting allowed the identification and survey of eight sites that were each marked with an alphabetic letter (A-H) (Figure 1B). The wrecks have been dated mainly from the pottery contexts: the first wreck discovered contained Dressel 20-shaped amphorae in its cargo and is dated to the 1st century AD; the second, dating back

to the 2nd century B.C., contained Greek-Italian amphorae. These ships were most likely stranded on the cliff following a shipwreck.

According to the information found in the wrecks, it is feasible to guess the routes the ships took based on the cargo they carried. For example, the wine amphorae and ceramics were likely shipped from southern Italy, whereas the shipment of fish sauce and oil was likely coming from Betica, Spain.

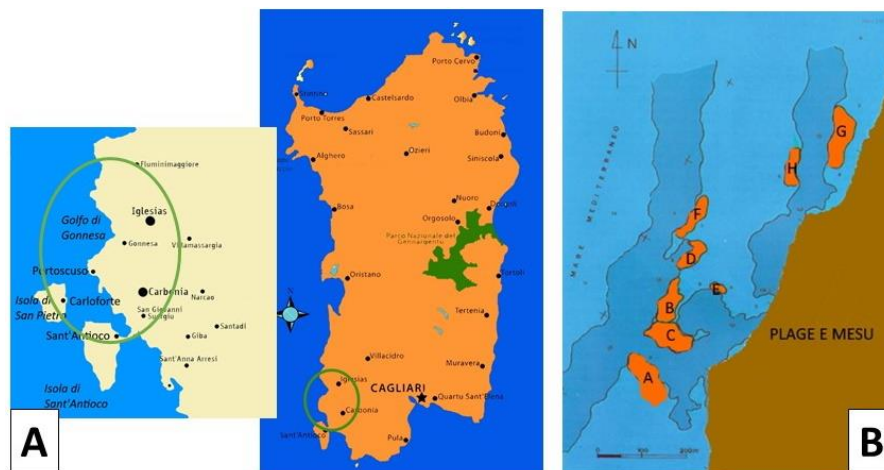


Figure 1. A) Map of Sardinia showing the location of Fontanamare Bay. B) Survey of discovery sites marked with an alphabetic letter (A-H).

With regard to the numismatic material, it was found in several stages and consists of a rather large agglomeration of coins called "pane I" (bread), another of smaller dimensions, "pane II," some groups of coins with concretions, and about two hundred loose coins [3].

"Pane I" consists of a compact nucleus of coins with dimensions of 140 x 115 mm, where on the external surfaces it is possible to read about 14 coins. On its external part, it is possible to observe a texture of a fabric weaving imprint on one side, which suggests that the coins at the time of the shipwreck were contained in a canvas sack. It is possible to still see remnants of the original sack's fibres on a few coins, which serves as confirmation of this (Figure 2).

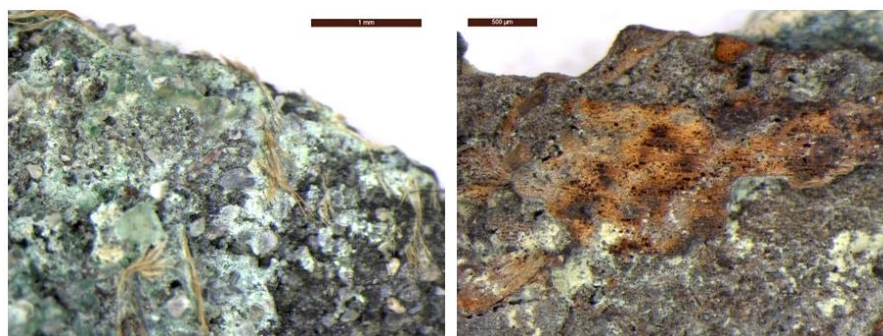


Figure 2. Optical images that show remnants of the original sack's fibres of the canvas sack.

The discovery of the coins has thus allowed us to attribute a certain date to the ship, although only a tiny number are clearly legible. Although the issuing authority cannot be determined with certainty due to the majority of the coins being either completely unreadable or fractured, it is certain that they are Antoninians coins from the third century AD.

But while the discovery of the coin is significant, its economic value is low; it was most likely a reserve of money intended for daily payments or sales profits. The fibres imprinting on one side of "Pane I" provides support for the hypothesis, implying that the coins were in a sack at the time of the shipwreck [2].

In this paper, nine bronze coins from the Fontanamare wreck were investigated for the first time using a multi-analytical approach combining optical microscopy (OM), micro-Raman (μ -Raman) spectroscopy, and X-ray diffractometry (XRD) to analyse the nature of the patina. Scanning electron microscopy with energy dispersive X-ray spectroscopy (SEM + EDS) was used to study the micro-structure of corrosion products and the nature of alloys by analysing the surface and cross-section [5].

Studies of the late Roman Empire Antoninians coins discovered in underwater archaeological sites can reveal details about their production. It is also significant for understanding the complex corrosion processes that take place in underwater conditions.

2. The marine environment corrosion

When a coin is immersed in seawater, its surface interacts with the marine environment, resulting in a very complex corrosive phenomenon, and in a short period, electrochemical mechanisms begin [6-11].

Seawater is the primary corrosive agent in marine corrosion because it is a complex solution of many dissolved ionic salts, as well as the presence of other compounds such as dissolved gases (O_2 , CO_2), suspended substances, and the results of biological action that increase corrosion rate.

Seawater temperature [12], the nature of marine currents, salinity, pH, environmental zone to which the metal is exposed, are important factors to determine what and how quickly corrosion occurs.

The following average parameters should be considered for the Sardinian seabed, which is the deposition environment of the coins analysed: salinity has an average value of 35‰, with greater values observed in localised places (38.6‰) and pH is between 7.5 and 8.4 [13].

Oxygen and carbon dioxide, produced during photosynthetic underwater activities, are the main dissolved gases in seawater. Because of the high concentration of dissolved oxygen, seawater is strongly oxidizing agent; however, it can turn reducing due to biological activity.

The most significant component determining the corrosion phenomena is the concentration of the dissolved oxygen, which is possible to associate with numerous environmental parameters such as oxidation processes, fluxes between sea and atmosphere, organisms respiration, and photosynthesis [4]. This parameter varies depending on the geographical location, as well as the depth and temperature of the water. The corrosion phenomenon becomes more active as the concentration of dissolved oxygen increases. When this parameter falls, for example, at the mud-water interface, the concentration of chloride ions rises.

The concentration of dissolved oxygen also affects biological colonisation, which takes place on the surface of the metal after a short time of being submerged. Over time, the surface of the metal is covered by biofilm primarily made of aerobic and anaerobic bacteria that might accelerate the corrosion [14, 15].

Generally, the marine bacteria strain responsible for microbial corrosion belongs to the sulphate-reducing bacteria group. These bacteria contribute to corrosion by first solubilizing the metal surface with their hydrogenases, then reducing the sulphate to sulphide, causing the dissolution of the metal. The biofilm developed by these bacteria increases with exposure time, and its heterogeneities are also responsible for localised metal surface inhomogeneity, which favours the corrosion process [13].

In order to better understand the role played by different chemical and physical parameters in the corrosion of bronze artefacts in an underwater environment, this study attempts to understand the nature of the patinas on the coins in relation to the specific parameter variation [16, 17].

2. Materials and Methods

2.1. The Antoninianus coins

The *Antoninianus* coins were introduced under the reign of Caracalla (*Marcus Aurelius Antoninus*), ca. 214–215 A.D. [18]. The first coinage contained a high percentage of silver. Then, due to a

severe debasement of the mint due to the political context, argentiferous bronze coins were produced until the beginning of the reign of Diocletian, when he reintroduced high-quality silver coinage in 294 A.D.

As a result of the economic crisis, the *Antoninianus* coinage, which originally had a coin with a high silver content (up to 80% Ag), gradually declined, hitting its lowest values during the reigns of *Gallienus* and *Aurelianus* (270–275 A.D.), and turned into a bronze coin with a very low silver content (about 2–3% Ag). Cu, Pb, and Sn concentrations subsequently rise after Ag content declines [19].

In order to better correlate and understand the corrosion processes in submarine conditions related to the microchemical and microstructural properties of the material buried, nine *Antoninianus* coins (Figure 3) from the Fontanamare wreckage have been selected based on the different patina chemical and morphological features.

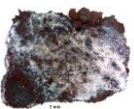
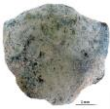
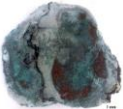


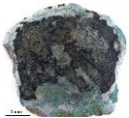



White-green patina coins			
F10	F26	F36	F40
			
Black patina coins			
F15	F16	F32	
			
Green patina coins			
F7	F14		
			

Figure 3. *Antoninianus* coins from Fontanamare wreckage analysed.

3.2. Analytical methods

The selected coins have been analysed by means of optical microscopy (OM), scanning electron microscopy (SEM) and energy dispersive X-Ray spectroscopy (EDS), X-ray diffraction (XRD) analysis, and micro-Raman (μ -Raman) spectroscopy.

Optical microscopy (OM) investigations were performed using a Leica M125 C microscope and a MEF 4 microscope equipped with a digital camera Leica MC170 HD.

SEM and EDS characterizations were carried out by a LEO VP 1450 equipped with a microprobe X-ray INCA 300 and a four-sector backscattered electron detector (BSE). The beam accelerating voltage was set between 20 and 30 keV sufficient to overcome the critical energy of the electrons for the X-ray emission (quantitative resolution limit of 0.2% by weight).

The structural identification of crystalline phases of the patinas was determined by a Siemens 5000 X-ray powder diffractometer using a Ni-filtered Cu K α radiation ($\lambda = 1.5418$). Angular values in the range between 10 and 80° in additive mode, a step size of 0.05°, and a sampling time of 2 s were the experimental parameters used for data acquisition. X-ray diffraction pattern analysis was carried out using electronic databases.

μ -Raman analysis was performed at room temperature using a Renishaw RM2000, equipped with a Peltier-cooled charge-coupled device (CCD) camera, in conjunction with a Leica optical microscope with $\times 10$, $\times 20$, $\times 50$ and $\times 100$ objectives. Measurements were performed using the $\times 50$ objective (laser spot diameter of about 1 μ m) and the 514.5 nm excitation line of an Ar⁺ laser using the equipped density filter and with a real output of 300 μ W.

3. Results

The characterization results of nine coins were chosen as the most representative of the three types of patinas identified: white, black, and green patinas. Figure 3 shows the morphological features of the selected coins.

3.1. White-green patina coins

The optical image of the F10 coin is shown in Figure 4 A. To analyse the microchemical and microstructural features of the surface layer, SEM/EDS analyses (Figures 4 B and D) were carried out. The SEM image shows a not uniform patina, with light and dark areas of different chemical compositions observed through backscattered electrons, as evidenced by the EDS spectra recorded on the A, B, and C areas, where Pb, Sn and Cu, Cl and S elements are respectively present.

The nature of the corrosion products was defined by means of the XRD analysis (Figure 4 C) and highlights the presence of Pb compounds like the lead carbonates cerussite (PbCO_3) and the lead oxide. The presence of Pb is related to the alloy composition of the Antoninianus coins, which held high levels of Pb.

Lead-containing corrosion products, like cerussite, may be more prevalent in the patina as a result of lead segregating to the outer surface of the mould during casting. When the bronze contains isolated globules of lead, similar segregation events can take place, and, over time, Pb migrates to the alloy surface, where it reacts with ions from the environment to form Pb compounds [20]. Moreover, lead acetates and basic carbonates can form when leaded bronze items are in contact with wooden or fibre composites, glues, rubbers, and other materials since lead is particularly susceptible to corrosion in the presence of organic acids [21]. The storage of Fontanamare coins in a sack at the time of the shipwreck may have made it easier for Pb corrosion products to form.

Furthermore, the diffractogram reveals the presence of silver, used as an alloying element in the manufacturing process of the *Antoninianus* coins.

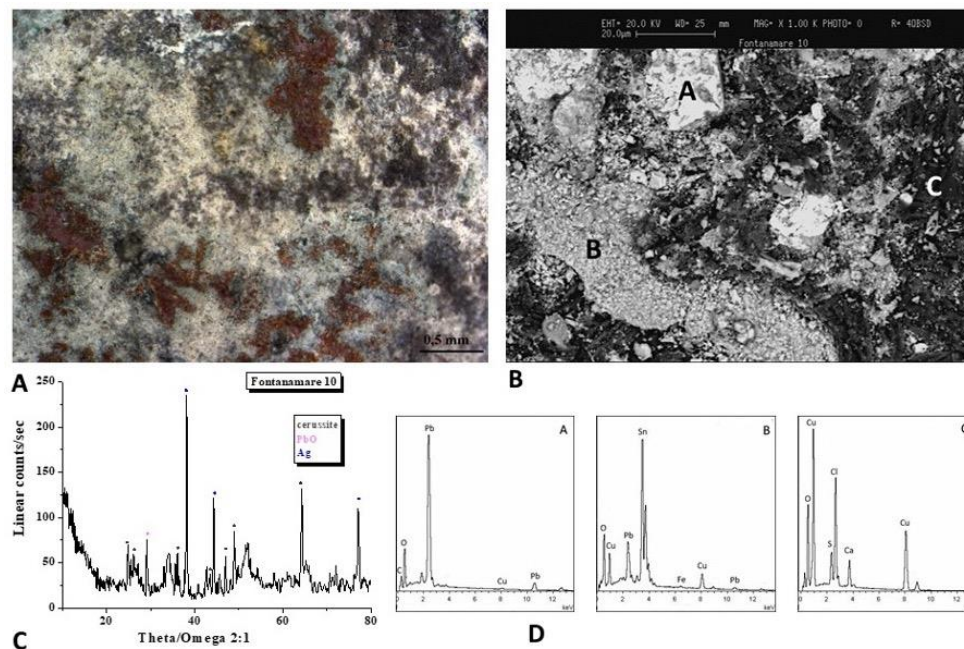


Figure 4. Surface analysis of coin F10: A, B) Optical images of coin surface. B) XRD analysis that highlights the presence of the lead carbonate cerussite (PbCO_3) and the lead oxide. D) EDS spectra recorded on the A, B, and C areas, where Pb, Sn and Cu, Cl and S elements are respectively present.

The optical image of the F26 coin is shown in Figure 5 A. The SEM image (Figure 5 B) shows a non-uniform patina with a white area rich of Pb, Cl and Sn and a dark area rich of Pb and Cl as evidenced by the EDS spectra (Figure 5 D).

The XRD analysis (Figure 5 C) defines the presence of cerussite as well as the lead chloro-carbonate phosgenite ($(\text{PbCl})_2\text{CO}_3$) formed when sea water is present as sources of chlorine.

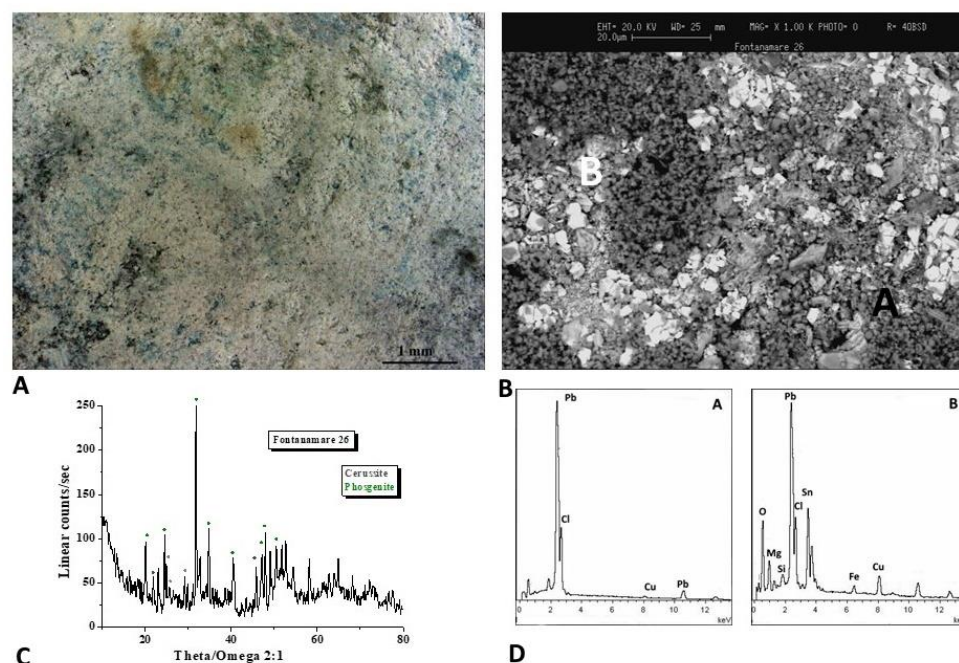


Figure 5. Surface analysis of coin F26. Characterizations of the artefacts: A, B) Optical images of coin surface. B) XRD analysis that highlights the presence of cerussite and phosgenite ($(\text{PbCl})_2\text{CO}_3$). D) EDS spectra recorded on the A, B areas, where Pb, Cl and Sn and a dark area rich of Pb and Cl elements are respectively present.

Figure 6 A shows the optical image of the F36 coin. The surface has a green and white patina that is primarily composed of Pb, Cu and Cl, with darker layers composed of soil minerals as evidenced by EDS spectra (Figures 6 B and D). The diffractogram (Figure 6 C) reveals the presence of atacamite ($\text{Cu}_2\text{Cl}(\text{OH})_3$), botallackite ($\text{Cu}_2(\text{OH})_3\text{Cl}$) and cuprite (Cu_2O). These corrosion products are frequently found on bronze artefacts that have been buried in marine environments [22].

The presence of copper chloride hydroxide (atacamite and botallackite) in the coin F36 suggests a change of the hydroxyl/chloride ratio in the solution. Even though nantokite (CuCl) has not been found, it is likely that it acted as a precursor to the formation of atacamite, resulting in the cyclic oxidation and hydrolysis reactions known as bronze disease [21]. It should be noted that the cuprite phase is stable at a pH range like that of seawater, which ranges between 6.2 and 9.2, according to the Pourbaix diagram for copper in oxygenated seawater at 25°C, while the formation of cuprous chloride from cuprite is not favoured [23]. As we said before, almost all saltwater has a pH that typically ranges around 8, however, significant variations can happen in limited areas such as beneath concretions, and cuprous chloride can be observed in seawater as a corrosion product if the local pH level is low enough to encourage its development.

Therefore, if erosion of the biofilm does not take place, the chloride ions present in the seawater will seep into the oxide film and interact with the metal, forming the dangerous cuprous chloride nantokite (CuCl). The CuCl film is then oxidised, resulting in atacamite and clinoatacamite ($3\text{Cu}(\text{OH})_2\text{CuCl}_2$). These are the main corrosion products of copper in a marine environment, and it is a very aggressive form of corrosion known as "bronze disease," which destroys the artefacts in a very short time.

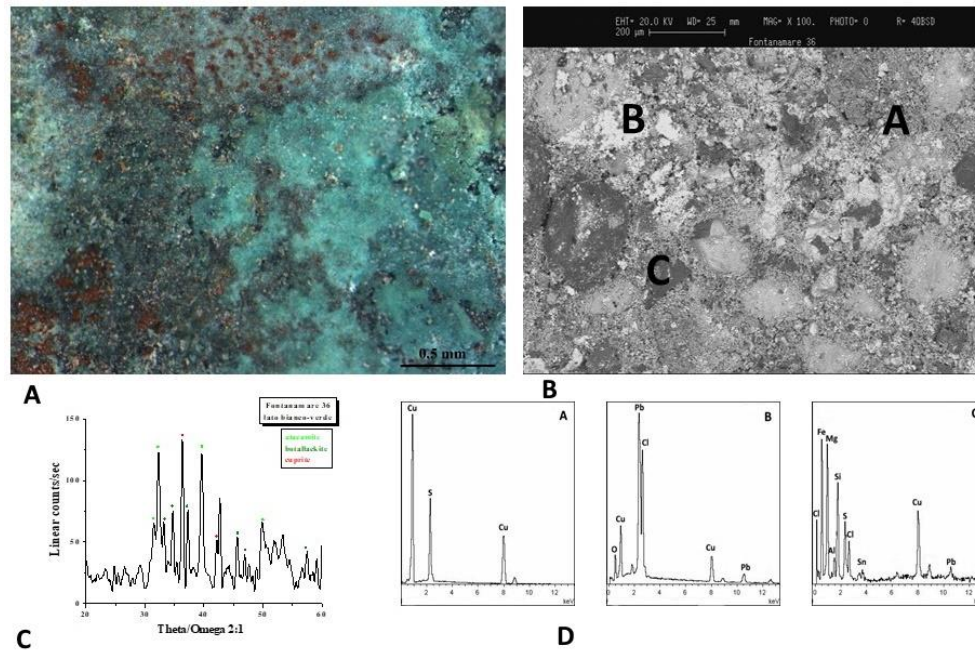


Figure 6. Surface analysis of coin F36. Characterizations of the artefacts: A, B) Optical images of coin surface. B) XRD analysis that highlights the presence of atacamite ($\text{Cu}_2\text{Cl}(\text{OH})_3$), botallackite ($\text{Cu}_2(\text{OH})_3\text{Cl}$) and cuprite (Cu_2O). D)EDS spectra recorded on the A, B and C areas, where of Pb, Cu and Cl elements are respectively present.

The optical image of the F40 coin is shown in Figure 7 A. According to SEM and EDS spectra (Figure 7 B and D), the brown-white patina is composed of Sn and Pb in the white region and Cu and Sn besides the soil components in the darker area. The diffractogram (Figure 6 C) shows that cassiterite (SnO_2) and cuprite (Cu_2O) are the predominant component of the surface layer.

The decuprification phenomenon, or the selective dissolution of the Cu, results in the surface of the alloy being enriched with Sn, which gives rise to cassiterite. The object is protected from corrosion by a passivation film formed when Sn oxidises on the surface [24].

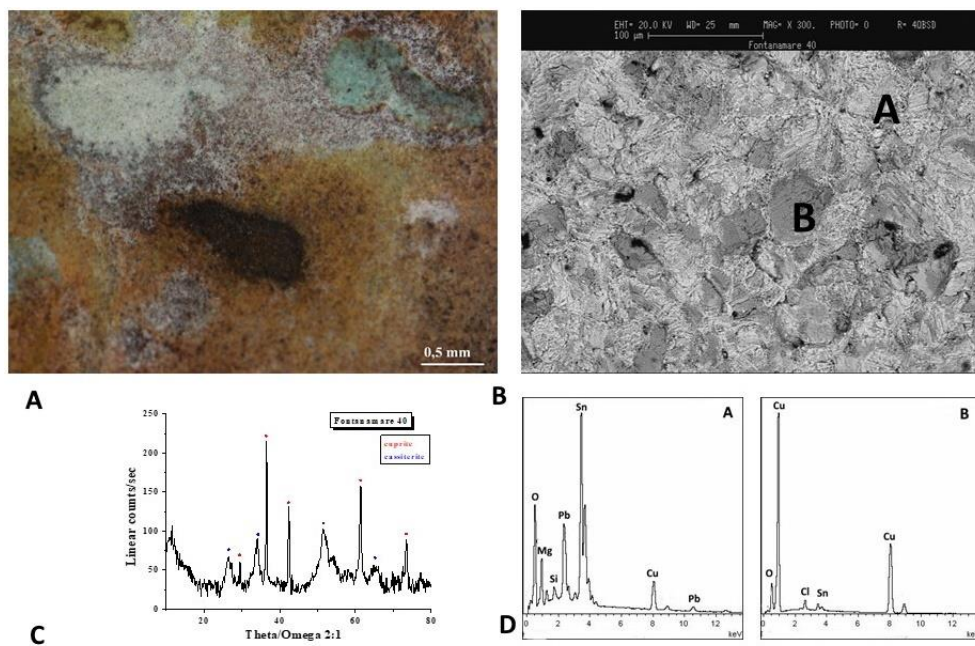


Figure 7. Surface analysis of coin F40. Characterizations of the artefacts: A, B) Optical images of coin surface. B) XRD analysis shows that cassiterite (SnO_2) and cuprite (Cu_2O) are the predominant component of the surface layer. D) EDS spectra highlights the brown-white patina composed of Sn and Pb in the white region and Cu and Sn besides the soil components in the darker area.

3.2. Black patina coins

The optical image of the F15 coin is shown in Figure 8 A. According to SEM and EDS spectra (Figure 8 B and C), the patina is composed of Cu and S in the predominantly black areas.

The nature of the corrosion products was defined by the XRD analysis and Raman spectra. The XRD pattern shown in Figure 8D provides further evidence that Cu_2S (chalcocite) formed as the primary component of the surface layer. The presence of additional copper sulphides, such as CuS (covellite), which form if the reactive sulphide anions are present, is revealed by the Raman spectrum of Figure 8 E, obtained in a darker region.

The corrosion products on bronze artefacts buried in the submarine environments can vary in composition from covellite to chalcocite (Cu_2S) [25]. In fact, sulphide ions are formed during burial conditions, where the reduction of sulphate ions by bacteria under anaerobic conditions can occur [26 - 29], and they can precipitate as copper sulphides with the copper ions coming from the artefacts. Because the copper sulphides can range in colour from greenish-black to blackish lead-grey to blue, the artefacts appearance can shift.

The process by which the copper sulphide is formed, as we have already mentioned, depends on a variety of factors, including the surface of the artefact, the sulphur content created by the decomposition of organic matter, and the nearly oxygen-free environment.

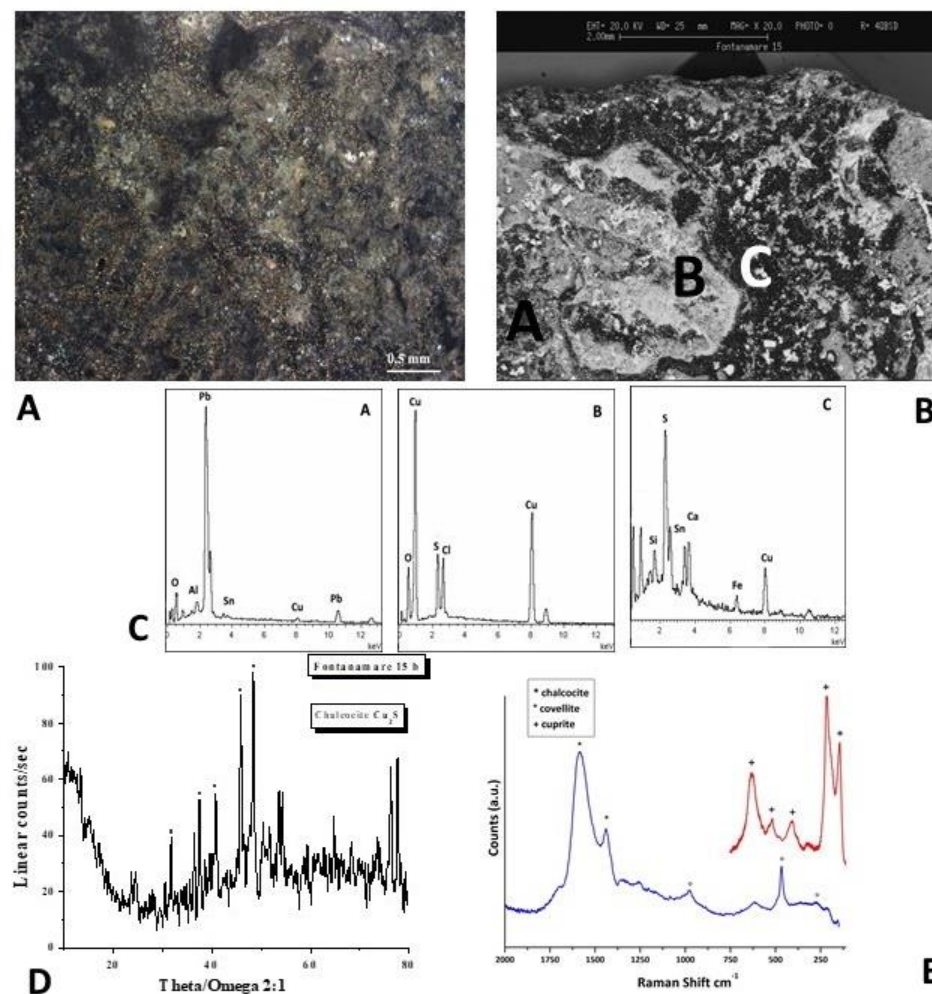


Figure 8. Surface analysis of coin F15. Characterizations of the artefacts: A, B) Optical images of coin surface C) EDS spectra highlight the patina is composed of Cu and S in the predominantly black areas. D) XRD analysis evidence that Cu_2S (chalcocite) formed as the primary component of the surface layer. E) Raman spectra reveal the presence of CuS (covellite) and Cu_2S (chalcocite).

The optical image of the F16 coin is shown in Figure 9 A. According to the EDS spectra (Figure 9 C), the patina is composed of Cu and S in the predominantly black areas.

Several characterisations were performed to identify the microchemical and microstructural features of the surface layer, whose nonuniformity is evident in the SEM image of Figure 9 B were brighter and darken areas are present. The EDS spectra recorded on the A, B, C and D areas, shown in Figure 9 C, also reveal the presence of Sn and Pb in brighter area, and Cu, Cl and S in darker areas.

The nature of the corrosion products was defined by the XRD analysis and Raman spectra. The XRD pattern and Raman spectra shown in Figures 9 D and E provide further evidence that Cu_9S_5 (roxbyite), covellite (CuS) and chalcocite (Cu_2S) formed as the primary component of the surface layer of the dark zone and cassiterite (SnO_2) and cerussite (PbCO_3) as the primary component of the surface layer of the bright zone. The presence of atacamite ($\text{Cu}_2\text{Cl}(\text{OH})_3$) is revealed by the Raman spectrum of Figure 9 E, obtained in a green region.

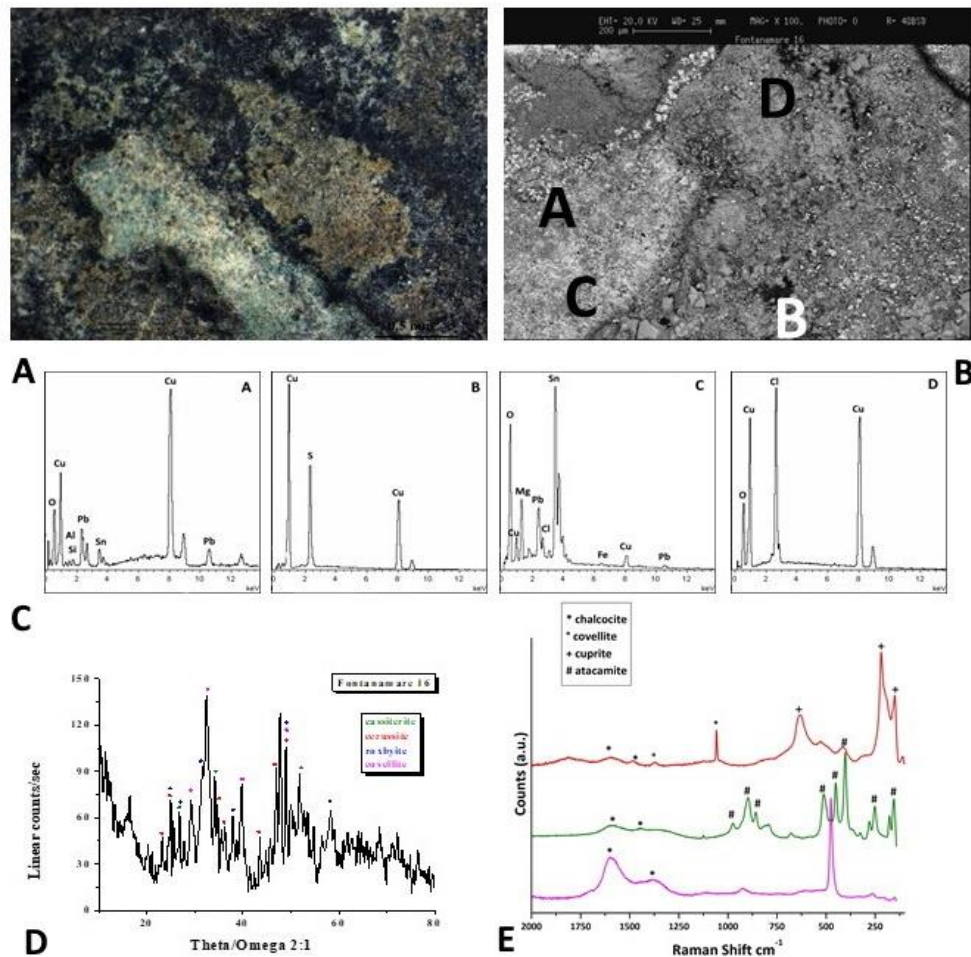


Figure 9. Surface analysis of coin F16. Characterizations of the artefacts: A, B) Optical images of coin surface. C) EDS spectra the patina is composed of Cu and S in the predominantly black areas and Sn and Pb in brighter area. D) XRD analysis evidence that Cu_9S_5 (roxbyite), covellite (CuS) and chalcocite (Cu_2S) formed as the primary component of the surface layer of the dark zone and cassiterite (SnO_2) and cerussite (PbCO_3) as the primary component of the surface layer of the bright zone. E) Raman spectrum reveals the presence of atacamite ($\text{Cu}_2\text{Cl}(\text{OH})_3$).

The optical image of the F32 coin is shown in Figure 10 A. According to the EDS spectra (Figure 10 D), the patina is composed of Cu and S in the predominantly black areas. The nature of the corrosion products is defined by the Raman spectra. The Raman spectra shown in Figure 10 C provide evidence that covellite (CuS) and chalcocite (Cu_2S) united to cuprite (Cu_2O) formed as the primary component of the surface layer.

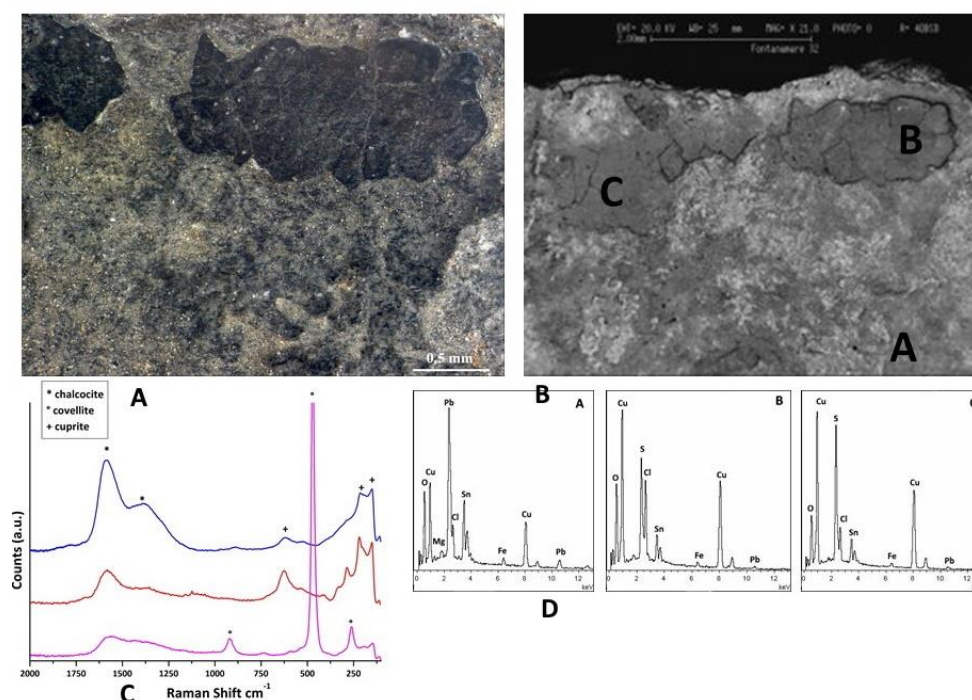


Figure 10. Surface analysis of coin F32. Characterizations of the artefacts: A, B) Optical images of coin surface. C) Raman spectrum covellite (CuS) and chalcocite (Cu_2S) united to cuprite (Cu_2O) formed as the primary component of the surface layer. D) EDS spectra the patina is composed Cu and S in the predominantly black areas.

The optical and SEM images of a metallographic section of F32 coin, shown in Figures 11 A and B, evidence the morphological details of the patina of the artefact. The EDS spectra (Figure 10 D) confirm a patina composed of copper sulphide, as confirmed by the Raman spectra (Figure 10 C); white areas are composed principally of Pb, and grey areas are composed of Cu, Sn, Cl, and Fe. The optical image evidences that the coin is almost completely mineralized.

In conclusion, the anaerobic conditions under the concretion created by biological colonisation can stimulate microbial induced corrosion (MIC), which would permit sulphate reducing bacteria to grow due to sulphate reducing bacteria (SRB) activity.

An artefact buried in anaerobic conditions favours the development of anaerobic microorganisms (SRB). Sulphate reduction is carried out by the SRB using sulphate as an electron acceptor. The oxidation of Cu combined with the reduction of sulphate is not thermodynamically favoured. So free Cu^+ ions are transformed into copper sulphides like chalcocite (Cu_2S), djurite ($\text{Cu}_{1.97}\text{S}$), and covellite (CuS) by the S created during their growth [30].

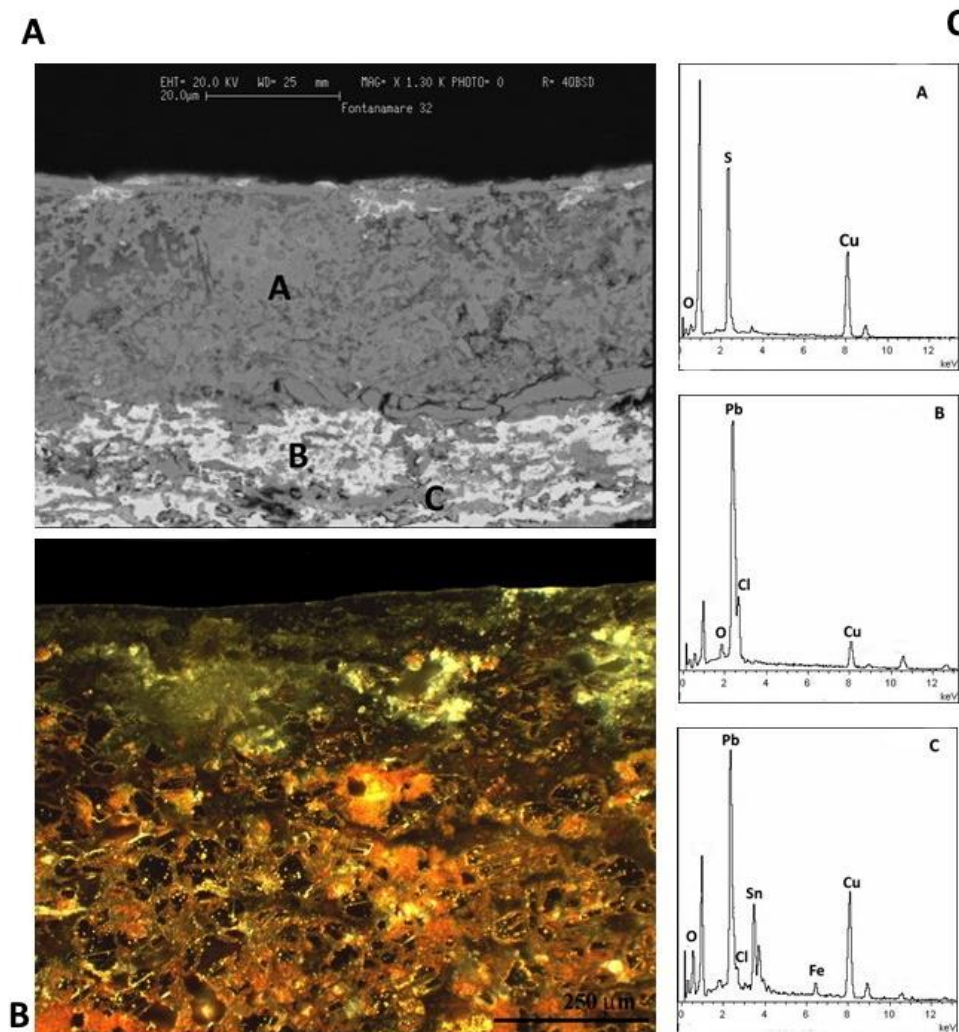


Figure 11. A,B) SEM and optical images of a metallographic section of F32 coin. C) EDS spectra confirm that the patina is composed of copper sulphide while white areas are composed principally of Pb, and grey areas are composed of Cu, Sn, Cl, and Fe. The optical image evidences that the coin is almost completely mineralized.

3.3. Green patina coins

The analytical results for the F7 and F14 coins are displayed in Figures 12 and 13 and 14. The surfaces have a stronger green patina that is predominantly made up of Pb, Cu, and Cl, as demonstrated by the EDS spectra in Figures 12 and 13 B. Botallackite ($\text{Cu}_2(\text{OH})_3\text{Cl}$) and atacamite-clinoatacamite ($\text{Cu}_2\text{Cl}(\text{OH})_3$) are both present, according to the diffractograms. Moreover, the EDS spectrum of F14 coins (Figure 13 D) reveals the presence of Ag on the coin's surface.

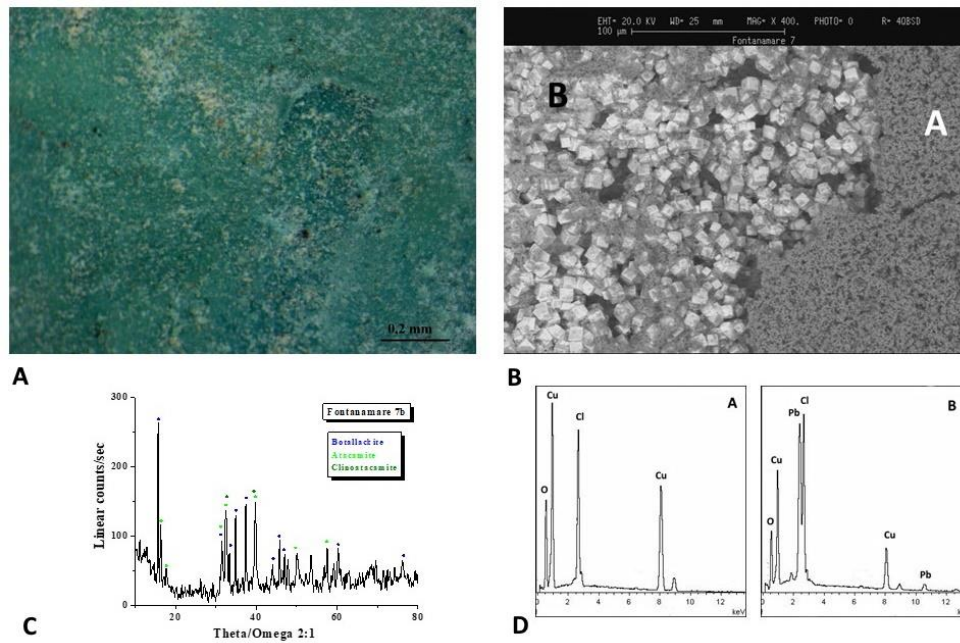


Figure 12. Surface analysis of coin F7. Characterizations of the artefacts: A, B) Optical images of coin surface. B) XRD analysis shows that botallackite ($\text{Cu}_2(\text{OH})_3\text{Cl}$) and atacamite-clinoatacamite ($\text{Cu}_2\text{Cl}(\text{OH})_3$) are the predominant component of the surface layer. D) EDS spectra highlights the presence of Pb, Cu, and Cl elements.

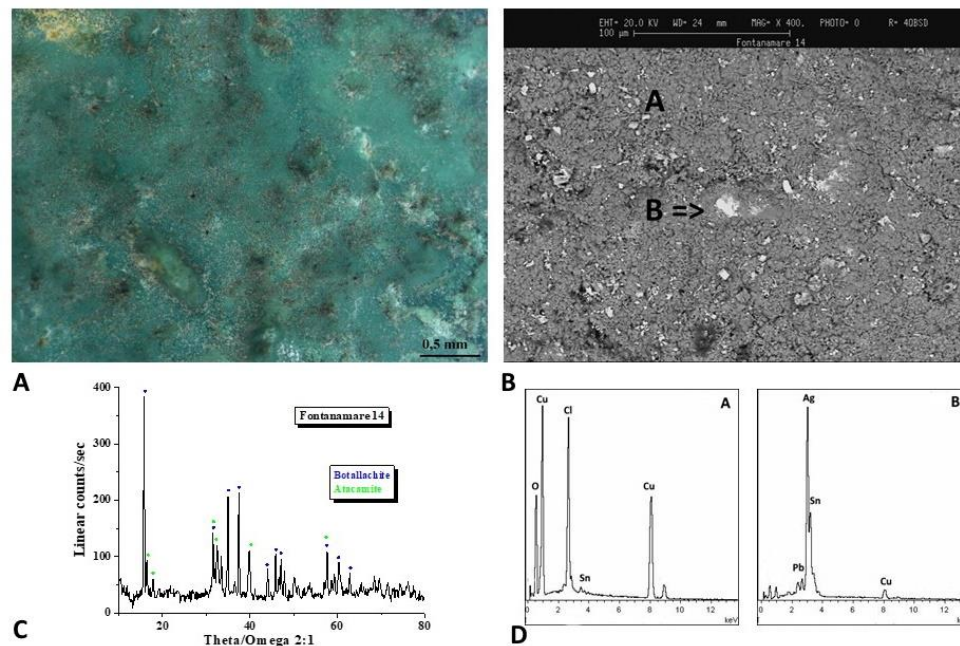


Figure 13. Surface analysis of coin F14. Characterizations of the artefacts: A, B) Optical images of coin surface. B) XRD analysis shows that botallackite ($\text{Cu}_2(\text{OH})_3\text{Cl}$) and atacamite-clinoatacamite ($\text{Cu}_2\text{Cl}(\text{OH})_3$) are the predominant component of the surface layer. D) EDS spectra highlights the presence of Pb, Cu, and Cl elements. Moreover, the EDS spectrum of F14 coins reveals the presence of Ag on the coin's surface.

The optical and SEM images of a metallographic section of F34 coin, shown in Figures 14 A and B, evidence the morphological details of the patina of the artefact.

As was previously observed from the surface study shown in Figure 13, the EDS spectrum (Figure 13 C, spectrum A) indicates that the external corrosion layer is composed of copper chloride hydroxide compounds [31].

EDS spectra in the outer region of the coin show a reduction in the Cu X-ray fluorescence signal close to the surface, confirming the decuprification of the alloy (Figure 13 C spectrum E). As a result, tin and silver enrichment occurs on the external surface. It should be noted that the content of Cu is low until 50 μm depth due to selective leaching. The alloy does not show visible corrosion at depths greater than 50 μm , below the boundary between the externally corroded layer and up to the inner core metal [32 - 34].

White Pb phases with elongated morphology can be identified in Figure 13 C, spectrum B. The fact that lead has no solid solubility in copper and copper-based alloys should also be considered. When lead in bronze alloy makes up more than a few percent of its weight, it appears as a dispersion of particles throughout the metal, and the number of these particles, known as globules, grows as the lead quantity increases [35 - 37].

Additionally, the cooling process of the alloy has a significant impact on the size and distribution of lead globules in the bronze artefacts. As a result, a leaded bronze object will not be uniform at the microscale, and the corrosion products that arise will have an extremely complicated microchemical structure.

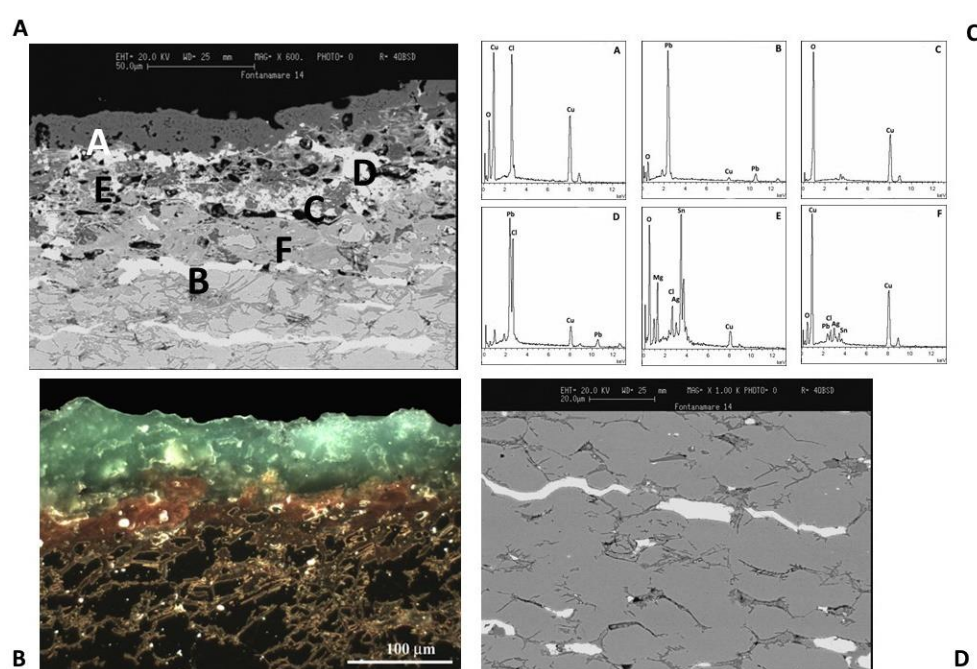


Figure 14. A,B) SEM and optical images of a metallographic section of F34 coin. C) EDS spectra indicates that the external corrosion layer is composed of copper chloride hydroxide compounds. The optical image evidences that the coin is almost completely mineralized. D) SEM image that evidence Pb phases with elongated morphology.

5. Conclusions

This study presents the first analysis of a group of coins from a Roman shipwreck that occurred off the coast of Fontanamare, Sardinia. This site is interesting since it has been a crossroads of Mediterranean trade routes since the Nuragic, Phoenician-Punic, and Roman times.

The purpose of this study has been to improve our knowledge of the commercial exchange that occurred in the period preceding Constantine and following the great economic crisis of the mid-3rd century AD, as well as to identify the deterioration processes that might impact metallic cultural heritage artefacts in submerged conditions.

By addressing queries about the peculiar deterioration mechanisms connected to soil characteristics and components, artefact chemical composition, and metallurgical aspects of the alloys, these investigations are able to reveal the complex microchemical nature of corrosion products. The coins have indeed different patinas, demonstrating how small variations in the chemical and physical parameters can influence the nature of the patina. The first group of coins, characterised by a white/green patina, revealed the presence of predominantly Pb compounds, which could have been formed by the interaction of the alloy's Pb content with the natural fibres of the sack that held the coins at the time of the shipwreck. The second group reveals a primarily black patina formed when bacteria reduce sulphate ions under anaerobic conditions. The final group of coins highlights the green patina and reveals the presence of hazardous copper chloride. The presence of chloride ions is thought to be dangerous because it triggers the copper cyclic corrosion reaction, which defaces the artefact and adversely affects its chemical-physical stability, as demonstrated in some case studies.

The analytical methodologies used have substantially benefited in identifying corrosion processes, permitting the development of specialised conservation strategies.

Finally, the metallographic section analysis confirmed the presence of a lead bronze with low silver content, the result of the severe economic crisis preceding the time of the Constantine government.

Author Contributions: Conceptualization, T.D.C. and A.M.; validation, T.D.C., A.M., M.L.R., and F.S.; investigation, T.D.C. and A.M.; resources, T.D.C.; data curation, T.D.C. and A.M.; writing—original draft preparation, T.D.C.; writing—review and editing, A.M., M.L.R.; visualization, A.M. and F.S.; supervision, T.D.C.; project administration, T.D.C.. All authors have read and agreed to the published version of the manuscript.

Funding: This research received no external funding

Data Availability Statement: Not applicable.

Acknowledgments: The authors acknowledge Claudio Veroli (ISMN-CNR) for XRD skilful technical assistance and Daniela Ferro for SEM helpful discussion.

Conflicts of Interest: The authors declare no conflict of interest.

References

1. Parker A.J. Artifact Distributions and Wreck Locations: The Archaeology of Roman Commerce. *Memoirs of the American Academy in Rome* **2008**, 6, 177-196.
2. Pallarés F. Fontanamare (Cagliari). Il relitto "A". *Bollettino di Numismatica* **2001**, 36-39, 9-151.
3. Faccenna F. Fontanamare (Cagliari). Il relitto "A". Il contesto monetale. *Bollettino di numismatica* **2001**, 36-39, 82- 126.
4. Estalayo E. Chemical study of degradation processes in ancient metallic materials rescued from underwater medium. *J. Raman Spectrosc.* **2019**, 50, 289-298. <https://doi.org/10.1002/jrs.5553>
5. Angelini E.; A. Batmaz; de Caro T; Faraldi F.; Grassini S.; Ingo G.M.; Riccucci C. The role of surface analysis in the strategies for conservation of metallic artefacts from the Mediterranean Basin. *Surf. Interface Anal.* **2014**, 46, 754–763. <https://doi.org/10.1002/sia.5512>
6. Farro N.W.; Veleva L.; Aguilar P. Copper Marine Corrosion: I. Corrosion Rates in Atmospheric and Seawater Environments of Peruvian Port. *The Open Corrosion Journal* **2009**, 2, 114-122. <https://doi.org/10.2174/1876503300902010130>
7. Veleva L; Farro N.W. Influence of seawater on copper patina composition. *Appl. Surf. Sci.* **2012**, 258, 10072–10076. <https://doi.org/10.1016/j.apsusc.2012.06.077>
8. Núñez L.; Reguera E.; Corvo F.; González E.; Vazquez C. Corrosion of copper in seawater and its aerosols in a tropical island. *Corros. Sci.* **2005**, 47, 461–484. <https://doi.org/10.1016/j.corsci.2004.05.015>
9. Cohen M.; Inberg A.; Dana Ashkenazi D.; Cvikel D. What You Clean Is What You Get: A Novel Chemical Cleaning Technique and the Interpretation of Corrosion Products Found in Late Roman Copper Alloy Coins Retrieved from the Sea. *Heritage* **2022**, 5, 3628–3647. <https://doi.org/10.3390/heritage5040189>
10. Crisci G.M.; La Russa M.F.; Macchione M.; Malagodi M.; Palermo, A.M.; Ruffolo S.A. Study of archaeological underwater finds: Deterioration and conservation. *Appl. Phys. A* **2010**, 100, 855–863. <https://doi.org/10.1007/s00339-010-5661-9>

11. Angelini E.; Grassini S.; Tusa S. Underwater Corrosion of Metallic Heritage Artefacts. *Corros. Conserv. Cult. Herit. Met. Artefacts* **2013**, 236–259. <https://doi.org/10.1533/9781782421573.3.236>
12. MacLeod I.D.; North N.A. 350 years of marine corrosion in Western Australia. *Corrosion Australasia* **1980**, 5, 3.
13. Elmouaden K.; Jodeh S.; Chaouay A.; Oukhrib R.; Salghi R.; Bazzi L.; Hilali M. Sulfate-Reducing Bacteria Impact on Copper Corrosion Behavior in Natural Seawater Environment. *Journal of Surface Engineered Materials and Advanced Technology* **2016**, 6, 36–46. <https://doi.org/10.4236/jseamat.2016.62004>
14. Little B.J.; Leeb J.S.; Rayc R.I. The influence of marine biofilms on corrosion: A concise review. *Electrochim. Acta* **2008**, 54, 2–7. <https://doi.org/10.1016/j.electacta.2008.02.071>
15. Bethencourt M.; Fernández-Montblanc T.; Izquierdo A.; González-Duarte M.M.; Muñoz-Mas C. a Study of the influence of physical, chemical and biological conditions that influence the deterioration and protection of Underwater Cultural Heritage. *Sci. Total Environ.* **2018**, 98–114. <https://doi.org/10.1016/j.scitotenv.2017.09.007>
16. Macchia A.; Colasanti I.A.; Rivaroli L.; Favero G.; de Caro T.; Pantoja Munoz L.; Campanella L.; La Russa M.F. Natural based products for cleaning copper and copper alloys artefacts. *Nat. Prod. Res.* **2023**, 37,7. <https://doi.org/10.1080/14786419.2021.2000408>
17. Randazzo L.; Ricca M.; Pellegrino D.; La Russa D.; Marrone A.; Macchia A.; Rivaroli L.; Enei F.; La Russa M.F. Anti-fouling additives for the consolidation of archaeological mortars in underwater environment: Efficacy tests performed on the apsidal fishpond of Castrum Novum (Rome, Italy). *International Journal of Conservation Science* **2020**, 11, 243–250. <https://creativecommons.org/licenses/by-nc-nd/4.0/>
18. Salvi D. Mercanti e imperatori: bolli, marchi e monete provenienti da scavi subacquei. In *Rivista elettronica di Archeologia e Arte*, Proceedings of Giornate di studio di archeologia e storia dell'arte a 20 anni dall'istituzione del Dipartimento di Scienze Archeologiche e Storico-artistiche dell'Università degli Studi di Cagliari, Cagliari, Italy, 1-5 march 2010; Dipartimento di Storia, Beni Culturali e Territorio dell'Università degli Studi di Cagliari Sezione di Archeologia e Storia dell'Arte Cittadella dei Musei - Piazza Arsenale 1, Cagliari, Italy.
19. Craddock P.T. The composition of the copper alloys used by the Greek, Etruscan and Roman civilizations. *J. Archaeol. Sci.* **1976**, 3, 93–113. [https://doi.org/10.1016/0305-4403\(76\)90079-0](https://doi.org/10.1016/0305-4403(76)90079-0)
20. Costa V.; Urban F. Lead and its alloys: metallurgy, deterioration and conservation. *Conservation* **2005**, 6, 48 – 62. <https://doi.org/10.1179/sic.2005.50.Supplement-1.48>
21. Scott D.A. *Copper in Art - Copper and Bronze in Art: Corrosion, Colorants, Conservation*; Getty Publications, Los Angeles, California, 2002.
22. North N.; MacLeod, I. Corrosion of metals. *Conserv. Mar. Archaeol. Objects* **1986**, 68–98. <https://doi.org/10.1016/B978-0-408-10668-9.50010-1>
23. Piccardo P.; Mille B.; Robbiola L. Tin and copper oxides in corroded archaeological bronzes. *Corros. Met. Herit. Artefacts* **2007**, 239–262. <https://doi.org/10.1533/9781845693015.239>
24. Robbiola L.; Blengino J.-M.; Fiaud C. Morphology and mechanisms of formation of natural patinas on archaeological Cu–Sn Alloys. *Corros. Sc.* **1998**, 40, 2083–2111. [https://doi.org/10.1016/S0010-938X\(98\)00096-1](https://doi.org/10.1016/S0010-938X(98)00096-1)
25. de Caro T.; Caschera D.; Ingo G.M.; Calandra P. Micro-Raman innovative methodology to identify Ag–Cu mixed sulphides as tarnishing corrosion products. *J. Raman Spectrosc.* **2016**, 47, 852–859. <https://doi.org/10.1002/jrs.4900>
26. Sánchez del Junco A.; Moreno D.A.; Ranninger C.; Ortega-Calvo J.J.; Sàiz- Jiménez C. Microbial induced corrosion of metallic antiquities and works of art: a critical review. *Int. Biodeter. Biodegr.* **1992**, 29, 367–375. [https://doi.org/10.1016/0964-8305\(92\)90053-Q](https://doi.org/10.1016/0964-8305(92)90053-Q)
27. MacLeod M.B.; Jones J.M.; Little B.J. Production of sulfide minerals by sulfate reducing bacteria during microbiologically influenced corrosion of copper. *Corrosion* **1991**, 47, 9,674–677.
28. Rémaizeilles, C.; Langlet-Marzloff V.; Creus J.; Lotte G.; Deshayes C.; Baleux F.; Robbiola L. Remarkable corrosion resumption of archaeological bronzes, induced by the oxidation of ternary Cu–Sn–S phases in atmosphere, after long-term burial with sulfides. *Corros. Sci.* **2020**, 175, 108865. <https://doi.org/10.1016/j.corsci.2020.108865>
29. Faraldi F.; Cortese B.; Caschera D.; Di Carlo G.; Riccucci C.; de Caro T.; Ingo G.M. Smart conservation methodology for the preservation of copper-based objects against the hazardous corrosion. *Thin Solid Films* **2017**, 622, 130–135. <https://doi.org/10.1016/j.tsf.2016.12.024>

-
30. Armetta F.; Ponterio R.C.; Pibiri I.; Saladino M.L. New Insight on Archaeological Metal Finds, Nails and Lead Sheathings of the Punic Ship from Battle of the Egadi Islands. *Molecules* **2023**, *28*, 1968. <https://doi.org/10.3390/molecules28041968>
 31. Scott, D.A. Bronze Disease: A review of some chemical problems and the role of relative humidity. *J. Am. Inst. Conser.* **1990**, *29*, 193–206. <https://doi.org/10.1179/019713690806046064>
 32. Oudbashi O.; Wanhill R. Long-Term Embrittlement of Ancient Copper and Silver Alloys. *Heritage* **2021**, *4*, 2287–2319. <https://doi.org/10.3390/heritage4030130>
 33. Armetta F.; Saladino M.L.; Scherillo A.; Caponetti E. Microstructure and phase composition of bronze Montefortino helmets discovered Mediterranean seabed to explain an unusual corrosion. *Sci. Rep.* **2021**, *11*, 23022. <https://doi.org/10.1038/s41598-021-02425-6>
 34. Oudbashi O.; Emami S.M.; Ahmadi H.; Davami P. Micro-stratigraphical investigation on corrosion layers in ancient Bronze artefacts by scanning electron microscopy energy dispersive spectrometry and optical microscopy. *Herit. Sci.* **2013**, *1*, 21. <https://doi.org/10.1186/2050-7445-1-21>
 35. Towarek A.; Mistewicz A.; Pilecka-Pietrusińska E.; Zdunek J.; Mizera J. Corrosion degradation of archaeological lead: A review and case study. *J. Archaeol. Sci. Rep.* **2022**, *45*, 103611. <https://doi.org/10.1016/j.jasrep.2022.103611>
 36. Griesser M.; Kockelmann W.; Hradil K.; Traum R. New insights into the manufacturing technique and corrosion of high leaded antique bronze coins. *Microchem. J.* **2016**, *126*, 181–193. <https://doi.org/10.1016/j.microc.2015.12.002>
 37. Doménech-Carbó M.T.; Di Turo F.; Montoya N.; Catalli F.; Doménech-Carbó A.; De Vito C. FIB-FESEM and EMPA results on Antoninianus silver coins for manufacturing and corrosion processes. *Sci. Rep.* **2018**, *8*, 10676. <https://doi.org/10.1038/s41598-018-28990-x>